Received: 2 May 2020 | Revised: 10 June 2020 | Accepted: 10 June 2020

DOI: 10.1111/jace.17320

ORIGINAL ARTICLE

Journal of the American Ceramic Society

Cold sintered $LiMgPO_4$ based composites for low temperature co-fired ceramic (LTCC) applications

Dawei Wang[1] | **Jinrong Chen**[2] | **Ge Wang**[1] | **Zhilun Lu**[1] | **Shikuan Sun**[1] | **Jinglei Li**[3] | **Juan Jiang**[1,4] | **Di Zhou**[3] | **Kaixin Song**[1,2] | **Ian M. Reaney**[1]

[1]Department of Materials Science and Engineering, University of Sheffield, Sheffield, UK

[2]College of Electronics Information, Hangzhou Dianzi University, Hangzhou, China

[3]Electronic Materials Research Laboratory, Key Laboratory of the Ministry of Education & International Center for Dielectric Research, School of Electronic Science and Engineering, Xi'an Jiaotong University, Xi'an, Shaanxi, China

[4]Faculty of Materials Science and Engineering, Hubei University, Wuhan, China

Correspondence
Dawei Wang, Kaixin Song, and Ian M. Reaney, Department of Materials Science and Engineering, University of Sheffield, Sheffield S1 3JD, UK.
Email: dawei.wang@sheffield.ac.uk (D. W.), k.song@sheffield.ac.uk (K. S.), i.m.reaney@sheffield.ac.uk (I. M. R.)

Funding information
Engineering and Physical Sciences Research Council, Grant/Award Number: EP/N010493/1 and EP/L017563/1

Abstract

Cold sintered, Li_2MoO_4-based ceramics have recently been touted as candidates for electronic packaging and low temperature co-fired ceramic (LTCC) technology but MoO_3 is an expensive and endangered raw material, not suited for large scale commercialization. Here, we present cold sintered temperature-stable composites based on $LiMgPO_4$ (LMP) in which the Mo (and Li) concentration has been reduced, thereby significantly decreasing raw material costs. Optimum compositions, $0.5LMP\text{-}0.1CaTiO_3\text{-}0.4K_2MoO_4$ (LMP-CTO-KMO), achieved 97% density at <300°C and 600 MPa for 60 minutes. Raman spectroscopy, X-ray diffraction, scanning electron microscopy, and energy dispersive X-ray mapping confirmed the coexistence of end-members, LMP, CTO, and KMO, with no interdiffusion and parasitic phases. Composites exhibited temperature coefficient of resonant frequency ~ –6 ppm/°C, relative permittivity ~9.1, and $Q \times f$ values ~8500 GHz, properties suitable for LTCC technology and competitive with commercial incumbents.

KEYWORDS
cold sintering, LTCC, microwave dielectric ceramics, phosphates

1 | INTRODUCTION

With the rapid development of wireless communications such as Wi-Fi, "Internet of Things", and 5G, the use of microwave (MW) dielectric ceramics in the manufacture of radio frequency (RF) components, such as filters, resonators, antennas, and substrates,[1–5] has dramatically increased. Miniaturization and integration of RF components for 5th generation (5G) technology in particular requires new materials with short delay times ($\varepsilon_r < 15$), lower dielectric loss (high MW quality factor, $Q \times f$), and near-zero temperature coefficient of resonant frequency (TCF).[1–5]

Dawei Wang and Jinrong Chen contributed equally to this work.

Traditional MW ceramics are sintered at high temperature (T > 1000°C) to impart strength, integrity, and to optimize the required physical properties,[6–9] but energy consumption and associated carbon emissions are substantial and high T limits the integration of low cost metal electrodes (Ag) and polymers. These limitations have led to the development of low temperature cofired ceramics (LTCCs, 700°C-950°C) and ultralow temperature cofired ceramics (ULTCCs, 400 ~ 700°C),[10–13] with many potential new materials for LTCC and ULTCC technology reported in systems based on molybdates, borates, phosphates, and tungstates.[14–24]

Cold sintering is a radical departure in sintering technology in comparison with LTCC and ULTCC and employs an aqueous phase and uniaxial pressure to densify ceramics at <300°C for shorter times (<2 hours) than conventional sintering.[25–43] The energy consumed by cold sintering is <50% of that used by its conventional counterpart,[6] facilitating integration with polymers and base metals and liberating RF design space for ceramics, previously forbidden by their high sintering temperatures. To date, there have been numerous cold sintered materials touted to show promise as potential replacements of LTCC and ULTCC but almost all are based on MoO_4^{2-}, eg refs 25, 26. Mo is an expensive and endangered raw material[44,45] not suited for mass production in the electronics sector, and new ceramics and composites are required that either eradicate or reduce the concentration of Mo if cold sintering is to compete for applications in MW technology.

Phosphates (PO_4^{3-}) are low cost in comparison to molybdates,[46,47] exhibit high $Q \times f$ (25 000~80 000) and low ε_r (<20),[20,21,22] when conventionally sintered at 800°C-1200°C and offer partial solubility in water, essential for cold sintering.[35,39] Although cold sintered phosphates have been reported, most have relatively low density and none have near-zero TCF.[48] In the present work, $LiMgPO_4$ (LMP, ε_r = 6.6, $Q \times f$ = 79 100, TCF = –55 ppm/°C)[20] is selected as a base to realize low cost, cold sintered (<300°C) composite ceramics to develop materials suitable for LTCC applications. 0.5LMP-0.1$CaTiO_3$-0.4K_2MoO_4 (LMP-CTO-KMO) composites densified at 250°C, exhibited TCF ~ –6 ppm/°C, ε_r ~ 9.1, and $Q \times f$ ~ 8500 GHz, properties superior to commercial LTCC incumbents based on glass-ceramic composites.[49]

2 | EXPERIMENTAL PROCEDURES

LMP powder was synthesized by conventional solid-state processing. Raw chemicals, Li_2CO_3 (99.9%, Sigma-Aldrich), MgO (99.9%, Sigma-Aldrich), and NH_6PO_4 (>99%, Sigma-Aldrich) were weighed according to the stoichiometric compositions and ball-milled 24 hours in isopropanol. The mixed powders were dried at 80°C and calcined 4 hours at 900°C. LMP powders were ball-milled to reduce particle size. KMO (95%) and CTO (>99%) powders were purchased from Sigma-Aldrich. For comparison, LMP was uniaxially pressed and conventionally sintered 2 hours at 950°C to obtain dense bulk ceramics.

1-2g of LMP, KMO, and CTO powders were weighed according to the formula of 50wt%LMP-10wt%CTO-40wt%KMO and then sufficiently mixed with 5-10wt%

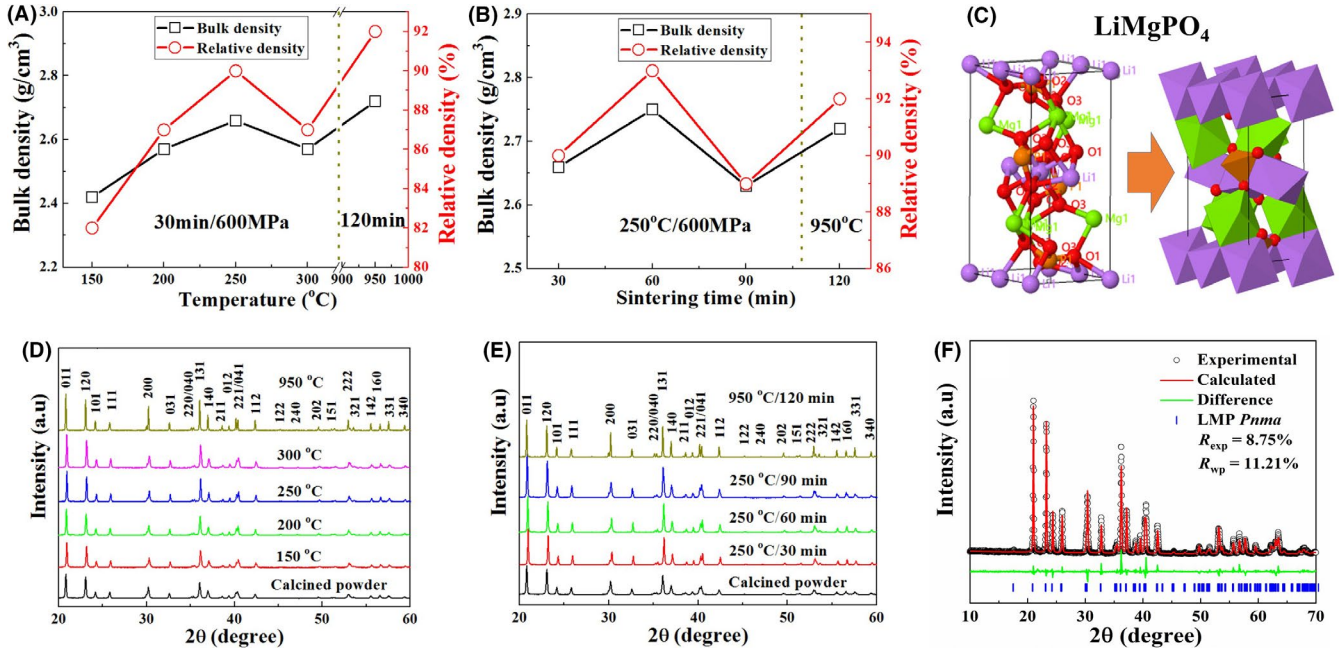

FIGURE 1 Bulk and relative density of LMP ceramics as a function of (A) sintering temperature and (B) sintering time. C, Schematic of the crystal structure of LMP. XRD patterns of LMP ceramics at different (D) sintering temperatures and (E) sintering times. F, Rietveld refinement of LMP ceramics cold sintered 60 min at 250°C [Color figure can be viewed at wileyonlinelibrary.com]

TABLE 1 Sintering condition, bulk density (ρ), relative density (ρ_r), and MW properties of LMP and LMP-CTO-KMO ceramics

Composition	Sintering condition	ρ (g/cm^3)	ρ_r (%)	ε_r	$tan\delta$	$Q \times f$ (GHz)
LMP	950°C/120min	2.72	92	6.4	0.00035	31,000
	150°C/30min/600MPa	2.42	82	5.4	0.0016	6,900
	200°C/30min/600MPa	2.57	87	5.8	0.0007	16,000
	250°C/30min/600MPa	2.66	90	6.1	0.0008	14,000
	300°C/30min/600MPa	2.57	87	6.0	0.001	11,000
	250°C/60min/600MPa	2.75	93	6.5	0.0007	16,000
	250°C/90min/600MPa	2.63	89	6.2	0.003	3,600
LMP-CTO-KMO	200°C/60min/600MPa	2.84	94.5	8.59	0.001	8,480
	250°C/60min/600MPa	2.92	97	9.1	0.001	8,500
	300°C/60min/600MPa	2.87	95.5	9.01	0.001	8,000

deionized water by using a pestle and mortar, after which cold sintered ceramics and composites were prepared by pressing (Atlas Heated Platens, Specac) 30-90 minutes at 600 MPa and 150°C-300°C depending on composition.

The geometric method was used to calculate the bulk density (ρ) of samples, as reported elsewhere.[25,26]The ceramic microstructure and grain morphology were examined by scanning electron microscopy (SEM, FEI Inspect F-50). The crystal structure and phase assemblage were determined by X-ray powder diffraction (XRD, Bruker D2 Phaser). Raman spectra were obtained using a Renishaw inVia Raman spectroscopy. The measurement of MW properties (ε_r, TCF, tanδ and $Q \times f$) was conducted by the $TE_{01\delta}$ mode with a vector network analyser (Advantest R3767CH), following previously defined protocols.[25,26] The cavity was heated by a Peltier device and the resonant frequency (f) was measured from 25°C to 85°C. The corresponding TCF values were obtained using the formula:

$$\mathrm{TCF} = \frac{f_T - f_{T_0}}{f_{T_0} \times (T - T_0)} \times 10^6 \quad (1)$$

where the f_T and f_{T_0} are the $TE_{01\delta}$ resonant frequencies at temperatures, T and T_0 respectively.

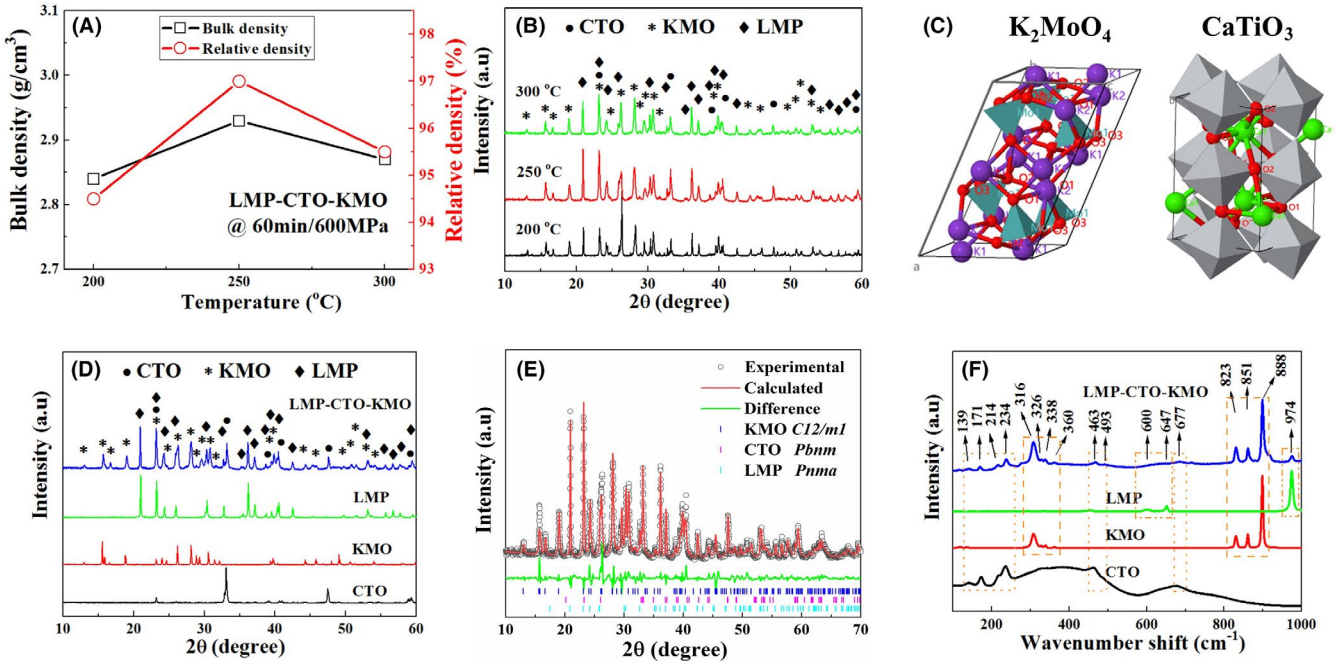

FIGURE 2 A, Bulk and relative density of cold sintered LMP-CTO-KMO composites as a function of sintering temperature. B, XRD patterns of cold sintered LMP-CTO-KMO composites at different sintering temperatures. C, Schematic of the crystal structures of KMO and CTO. D, XRD patterns of cold-sintered LMP-CTO-KMO, LMP, and KMO and commercial CTO powder. E, Rietveld refinement of cold sintered LMP-CTO-KMO composites. F, Raman spectra of cold-sintered LMP-CTO-KMO, LMP, and KMO and commercial CTO powder [Color figure can be viewed at wileyonlinelibrary.com]

3 | RESULTS AND DISCUSSION

The values of density (ρ) and relative density (ρ_r) for cold-sintered LMP ceramics are plotted in Figure 1A,B and listed in Table 1. As sintering temperature increases, the values of ρ and ρ_r both increase from 2.42 g/cm^3 (82%) at 150°C to 2.66 g/cm^3 (90%) at 250°C, followed by a decrease for higher sintering temperatures (Figure 1A). The optimum cold sintering temperature is therefore, 250°C. Sintering time at 250°C is subsequently increased and ρ and ρ_r is further optimized to 2.73 g/cm^3 (93%) for samples cold-sintered 60 minutes (Figure 1B). The maximum values of ρ ~ 2.73 g/cm^3 and ρ_r ~ 93% for cold-sintered LMP are higher than those reported for conventionally sintered LMP, (2.72 g/cm^{3}and 92%) (Figure 1B), illustrating the great promise of cold sintered LMP as a base to develop new materials.

Room-temperature XRD patterns of LMP calcined powders, conventionally sintered ceramics, and cold-sintered samples are shown in Figure 1D,E. LMP has a Mg_2SiO_4-type olivine structure (space group: *Pnma*, ISCD collection code: 201 138) and is composed of PO_4 tetrahedra and Li/MgO_6 octahedra (Figure 1C). Only diffraction peaks associated with olivine-structured LMP are detected in the XRD patterns (Figure 1D,E) with no impurity phases. Full-pattern Rietveld refinement of XRD data for LMP ceramics cold-sintered 60 minutes at 250°C was conducted using a Topas 5 software. The calculated pattern is in good agreement, with low values of $R_{exp} = 8.75\%$ and $R_{wp} = 11.21\%$, Figure 1F. The calculated lattice parameters are $a = 10.7418$ Å, $b = 5.9070$ Å, $c = 4.6909$ Å for LMP, which agree with those previously reported.[20]

The data presented above confirms that LMP may be cold sintered to moderately high density (93%) but further improvements were not obtained in the current study. Moreover, LMP has a large negative TCF (–55 ppm/°C) that falls outside excepted values for LTCC and ULTCC (+/–30 ppm/°C) applications. To adjust TCF closer to zero and to improve density, a bespoke cold sintering flux, 0.8KMO-0.2CTO (TCF = +70 ppm/°C) was developed based on KMO (TCF = –70 ppm/°C) but with a large positive TCF, adjusted through adding CTO (+850 ppm/°C).[25] Forming composites in this manner is typically used in commercial LTCC which

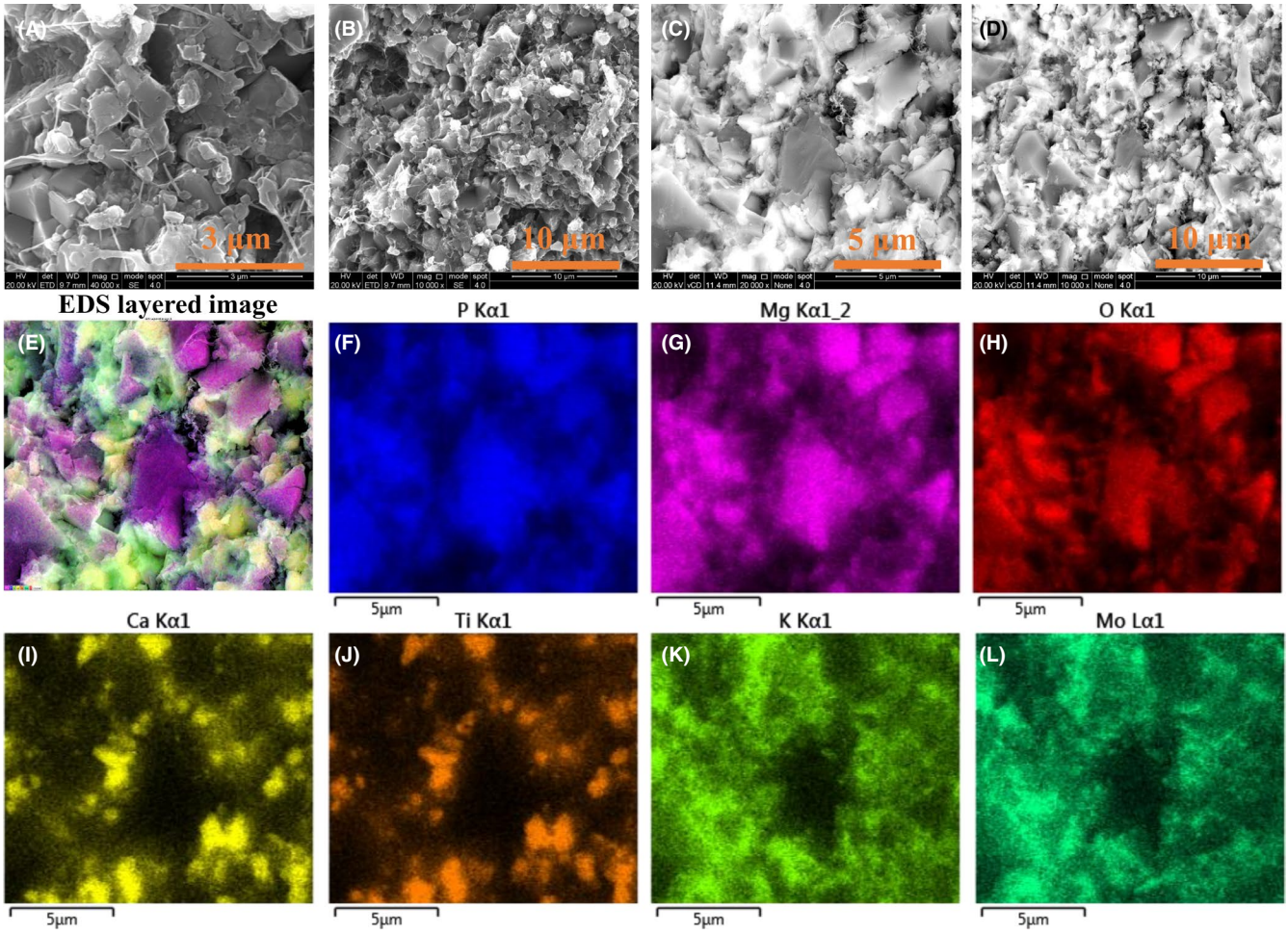

FIGURE 3 A and B, SEM images of LMP ceramics cold-sintered 60min at 250°C/600MPa. C and D, BSE images of LMP-CTO-KMO composites cold-sintered 60min at 250°C//600MPa. EDS mapping of LMP-CTO-KMO: (E) layered image, (F) P, (g) Mg, (H) O, (I) Ca, (J) T, (K) K, (L) Mo [Color figure can be viewed at wileyonlinelibrary.com]

are composed of a low melting temperature glass matrix with negative TCF and high ε_r, positive TCF phases such as TiO_2.[49]

ρ and ρ_r for cold-sintered LMP-CTO-KMO composites as a function of sintering temperature are plotted in Figure 2A and listed in Table 1. As sintering temperature increases to 200°C and 250°C, ρ and ρ_r increase to 2.84 g/cm^3 (94.5%) and 2.92 g/cm^3 (97%), respectively, followed by a slight decrease at higher sintering temperatures.

Room-temperature XRD patterns of cold-sintered LMP-CTO-KMO composites are shown in Figure 2B,D which reveal little change in phase assemblage as a function of sintering temperature. Only peaks from each end member are present: CTO exhibits an orthorhombic, perovskite structure (*Pbnm*, ISCD collection code: 62149); KMO is monoclinic (*C12/m1*, ISCD collection code: 16154) and LMP is as described in Figure 1. There is no evidence of secondary phases. Rietveld refinement was performed using a three-phase mix of LMP (*Pnma*), KMO (*C12/m1*), and CTO (*Pbnm*). The calculated pattern matches well with experimental data ($R_p = 9.65\%$ and $R_{wp} = 12.92\%$), where the weight fractions (LMP ~ 49.9%, CTO ~ 10.6%, KMO ~ 39.5%) are close to the nominal compositions, as shown in Figure 2E.

To confirm further the coexistence of three phases in composites, Raman spectra of cold-sintered LMP-CTO-KMO samples are shown in Figure 2F. As reported previously, 36, 10, and 39 Raman bands are commonly observed in LMP, CTO, and KMO respectively.[25,50,51] For LMP, there are 18 external modes (<400 cm^{-1}, 12 translations of Li, Ni, PO_4 tetrahedra, six vibrations of PO_4 tetrahedra), and 18 internal modes of PO_4 tetrahedra (>400 cm^{-1}, P-O stretching: $\nu_1 = 974$ cm^{-1}, $\nu_3 = 1020$-1080 cm^{-1}, O-P-O bending and P vibration: $\nu_2 = 416$-468 cm^{-1}, $\nu_4 = 590$-650 cm^{-1}), Figure S1. For CTO, Raman bands of 630 and 678 cm^{-1} are related to symmetric stretching of Ti-O. The 463 and 493 cm^{-1} bands are the torsional modes of Ti-O. The bands of 171, 214, 234, 275, and 323 cm^{-1} are related to the bending of O-Ti-O. The 139 cm^{-1} band belongs to the Ca ions motion. For KMO, Raman bands in the range of 100 ~ 160 cm^{-1} correspond to a combination of the translations and vibrations of MoO_4 tetrahedra and translations of K ions. The 310 ~ 370 cm^{-1} bands are related to bending modes of MoO_4 tetrahedra. The 820 ~ 890 cm^{-1} bands are related to stretching modes of MoO_4 tetrahedra. Raman spectra of LMP-CTO-KMO composites therefore, represent an overlay of Raman bands from individual phases, confirming the existence of LMP, KMO and CTO but without a significant volume fraction of interaction (Figure 2F).

SEM and BSE images of cold-sintered LMP ceramics and cold-sintered LMP-CTO-KMO composites are shown in Figure 3A,B and Figure 3C,D respectively. A denser microstructure in LMP-CTO-KMO composites than in LMP ceramics is evident, coincident with the higher density listed in Table 1. The variations in contrast in BSE images of LMP-CTO-KMO suggest that there are three chemically discrete CTO, KMO, and LMP rich phases, confirmed by the EDS mapping (Figure 3E-L).

The MW dielectric properties of LMP ceramics and LMP-CTO-KMO composites as a function of sintering temperature and time are presented in Figure 4 and listed in Table 1. As sintering temperature and time increase, ε_r and $Q \times f$ of LMP increases initially before decreasing. The highest values of $\varepsilon_r \sim 6.5$ and $Q \times f \sim 16\,000$ are achieved for LMP cold sintered 60 min at 250°C under a uniaxial pressure of 600 MPa

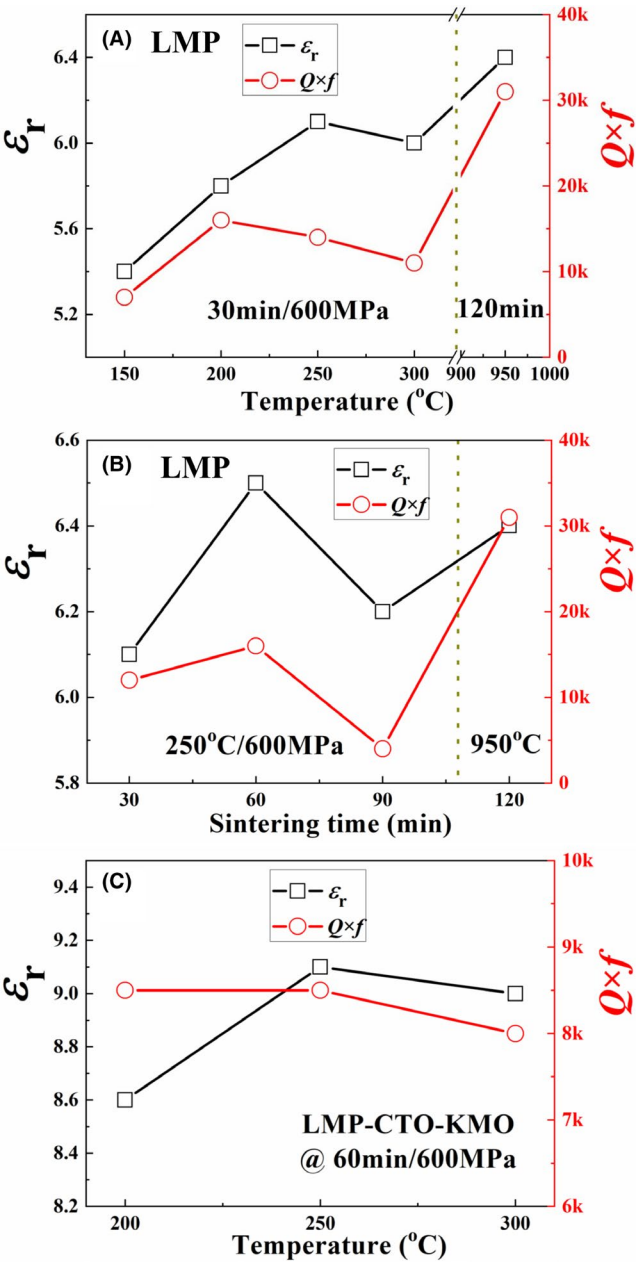

FIGURE 4 The microwave dielectric properties of LMP as a function of (A) sintering temperature (B) sintering time; (C) The microwave dielectric properties of LMP-CTO-KMO as a function of sintering temperature [Color figure can be viewed at wileyonlinelibrary.com]

TABLE 2 Comparison of sintering temperature (ST) and MV properties of LMP ceramics and LMP-CTO-KMO composites with other LTCCs

Compounds	ST (°C)	ε_r	$Q \times f$ (GHz)	TCF (ppm/°C)	Ref.
$CaZrO_3$+glass (Murata)	<1000	25	3500	<+/–30	49
Nd_2O_3-TiO_2-SiO_2+glass (NEC)	<1000	18	1200	<+/–30	49
Al_2O_3-$CaZrO_3$+glass (Dupont)	<1000	7.8	900	<+/–30	49
SiO_2-Al_2O_3-cordierite+glass (Kyocera)	<1000	5	8,000	<+/–30	49
LMP	950	6.6	79 100	–55	20
$(Bi_{0.05}Ce_{0.95})VO_4$	950	11.9	22 360	+6.6	19
$Bi_2(Li_{0.5}Ta_{1.5})O_7$+2%$Bi_2O_3$	920	64.1	11 200	–19	12
$Bi(Sc_{1/3}Mo_{2/3})O_4$	915	24.4	48 100	–68	15
0.45$BiVO_4$-0.55TiO_2	900	86	9500	–8	10
$Ca_{0.66}Bi_{0.34}Mo_{0.66}V_{0.34}O_4$	870	21.9	18 150	+0.1	18
$Li_6B_4O_9$	640	5.95	41 800	–72	17
$K_{0.5}(Nd_{0.6}Bi_{0.4})_{0.5}MoO_4$	620	17.3	13 050	+4	16
$(Na_{1.2}Ag_{0.8})MoO_4$	410	8.1	44 800	–82	14
LMP	250	6.5	16 000	–58	This work
LMP-CTO-KMO	250	9.1	8,500	–6	This work

(Figure 4A,B). The same conditions resulted in optimized values of cold sintered LMP-CTO-KMO composites with $\varepsilon_r \sim 9.1$, $Q \times f \sim 8500$ and a near zero TCF ~ –6 ppm/°C (Figure 4C).

The comparison of sintering temperature and MW properties for recently reported and commercial LTCCs are listed in Table 2. LMP-CTO-KMO composites exhibit the lowest sintering temperature (250°C), reducing energy costs in manufacture and ensuring compatibility with all low-cost electrode systems. $Q \times f$ of cold-sintered LMP-CTO-KMO composites are is superior to commercial LTCCs, ε_r is ideal and they are temperature stable (<+/–30 ppm/°C).[49] Cold sintering does not result in lateral shrinkage and hence issues relating to dissimilar shrinkage and thermal expansion between electrode and substrate are alleviated. Many materials are reported with higher $Q \times f$ and ε_r but these have not been commercialized due to either TCF> +/–30 ppm/°C, sintering temperature >900°C, high cost and environmental issues (Mo and V based systems) or they are over designed for the application; metallized LTCCs do not require ultra-high $Q \times f$ as losses are dominated by the metal/ceramic interface. Cold sintered LMP-CTO-KMO, therefore, satisfies the criteria for LTCC applications but we note that the production of cold sintered LTCC requires a radical rethink of ceramic processing and scale-up.

4 | CONCLUSIONS

Microwave LMP ceramics and LMP-CTO-KMO ceramic composites were successfully fabricated by cold sintering. As sintering temperature and time increase, ρ and ρ_r for LMP increased from 2.42 g/cm^3 (82%) at 150°C/30 min to 2.73 g/cm^3 (93%) at 250°C/60 min for which ε_r and $Q \times f$ was ~ 6.5 and ~ 16,000 GHz respectively. At the same sintering conditions, $\rho \sim 2.92$ g/cm^3 (97%), $\varepsilon_r \sim 9.1$, $Q \times f \sim 8500$, and near zero TCF ~ –6 ppm/°C were obtained for cold sintered LMP-CTO-KMO composites. LMP-CTO-KMO cold sintered composites were therefore considered suitable for LTCC applications.

ACKNOWLEDGMENT

This work was supported by EPSRC (EP/N010493/1 and EP/L017563/1).

ORCID

Dawei Wang https://orcid.org/0000-0001-6957-2494
Ge Wang https://orcid.org/0000-0003-1842-8067
Zhilun Lu https://orcid.org/0000-0002-9967-5221
Shikuan Sun https://orcid.org/0000-0002-1688-5072
Kaixin Song https://orcid.org/0000-0002-4622-1234

REFERENCES

1. Reaney IM, Iddles D. Microwave dielectric ceramics for resonators and filters in mobile phone networks. J Am Ceram Soc. 2006;89(7):2063–72.
2. Matin MA. Review on millimeter wave antennas-potential candidate for 5G enabled applications. Adv Electromag. 2016;5(3):98–105.
3. Ohsato H, Tsunooka T, Kan A, Ohishi Y, Miyauchi Y, Tohdo Y, et al. Microwave-millimeterwave dielectric materials. Key Eng Mater. 2004;269:195–8.
4. Albreem MA. 5G wireless communication systems: vision and challenges. Proceedings of the 2015 International Conference on Computer, Communications, and Control Technology (I4CT). Kuching, Malaysia: IEEE; 2015: p. 493–97. [Proceedings paper – published].

5. Fujii T, Ando A, Sakabe Y. Characterization of dielectric properties of oxide materials in frequency range from GHz to THz. J Eur Ceram Soc. 2006;26(10–11):1857–60.
6. Ibn-Mohammed T, Randall CA, Mustapha KB, Guo J, Walker J, Berbano S, et al. Decarbonising ceramic manufacturing: a techno-economic analysis of energy efficient sintering technologies in the functional materials sector. J Eur Ceram Soc. 2019;39(16):5213–35.
7. Lin Q, Song K, Liu B, Bafrooei HB, Zhou DI, Su W, et al. Vibrational spectroscopy and microwave dielectric properties of $AY_2Si_3O_{10}$ (A= Sr, Ba) ceramics for 5G applications. Ceram Int. 2020;46(1):1171–7.
8. Song Z, Song K, Liu B, Zheng P, Barzegar Bafrooei H, Su W, et al. Temperature-dependent dielectric and Raman spectra and microwave dielectric properties of gehlenite-type $Ca_2Al_2SiO_7$ ceramics. Int J App Ceram Tech. 2020;17(2):771–7.
9. Tan Z, Song K, Bafrooei HB, Liu B, Wu J, Xu J, et al. The effects of TiO_2 addition on microwave dielectric properties of $Y_3MgAl_3SiO_{12}$ ceramic for 5G application. Ceram Int. 2020;46(10):15665–9.
10. Zhou D, Guo D, Li WB, Pang LX, Yao X, Wang DW, et al. Novel temperature stable high-εr microwave dielectrics in the Bi_2O_3-TiO_2-V_2O_5 system. J Mater Chem C. 2016;4(23):535753–62.
11. Zhou D, Li J, Pang LX, Chen GH, Qi ZM, Wang DW, et al. Crystal structure, infrared spectra, and microwave dielectric properties of temperature-stable zircon-type (Y, Bi)VO_4 solid-solution ceramics. ACS Omega. 2016;1(5):963–70.
12. Zhou D, Pang LX, Wang DW, Li C, Jin BB, Reaney IM. High permittivity and low loss microwave dielectrics suitable for 5G resonators and low temperature co-fired ceramic architecture. J Mater Chem C. 2017;5(38):10094–8.
13. Hao S-Z, Zhou DI, Hussain F, Liu W-F, Su J-Z, Wang D-W, et al. Structure, spectral analysis and microwave dielectric properties of novel x $(NaBi)_{0.5}MoO_4$-(1–x)$Bi_{2/3}MoO_4$ (x=0.2∼0.8) ceramics with low sintering temperatures. J Eur Ceram Soc. 2020;40(10):3569–76.
14. Zhou D, Li J, Pang LX, Wang DW, Reaney IM. Novel water insoluble $(Na_xAg_{2-x})MoO_4$ (0≤ x≤ 2) microwave dielectric ceramics with spinel structure sintered at 410 degrees. J Mater Chem C. 2017;5(24):6086–91.
15. Zhou DI, Pang L-X, Wang D-W, Guo H-H, Yang F, Qi Z-M, et al. Crystal structure, impedance and broadband dielectric spectra of ordered scheelite-structured $Bi(Sc_{1/3}Mo_{2/3})O_4$ ceramic. J Eur Ceram Soc. 2018;38(4):1556–61.
16. Pang LX, Zhou D, Wang DW, Zhao JX, Liu WG, Yue ZX, et al. Temperature stable $K_{0.5}(Nd_{1-x}Bi_x)_{0.5}MoO_4$ microwave dielectrics ceramics with ultra-low sintering temperature. J Am Ceram Soc. 2018;101(5):1806–10.
17. Zhou D, Pang LX, Wang DW, Qi ZM, Reaney IM. High quality factor, ultralow sintering temperature $Li_6B_4O_9$ microwave dielectric ceramics with ultralow density for antenna substrates. Acs Sustain Chem Eng. 2018;6(8):11138–43.
18. Guo HH, Zhou D, Pang LX, Qi ZM. Microwave dielectric properties of low firing temperature stable scheelite structured (Ca,Bi)(Mo,V)O_4 solid solution ceramics for LTCC applications. J Eur Ceram Soc. 2019;39(7):2365–73.
19. Guo HH, Zhou D, Liu WF, Pang LX, Wang DW, Su JZ, et al. Microwave dielectric properties of temperature-stable zircon-type (Bi,Ce)VO_4 solid solution ceramics. J Am Ceram Soc. 2020;103(1):423–31.
20. Thomas D, Sebastian MT. Temperature-compensated $LiMgPO_4$: a new glass-free low-temperature cofired ceramic. J Am Ceram Soc. 2010;93(11):3828–31.
21. Zhang P, Wu S, Xiao M. The microwave dielectric properties and crystal structure of low temperature sintering $LiNiPO_4$ ceramics. J Eur Ceram Soc. 2018;38(13):4433–9.
22. Bian J, Sun X, Xie Y. Structural evolution, sintering behavior and microwave dielectric properties of $Al_{(1-x)}(Si_{0.5}Zn_{0.5})_xPO_4$ ceramics. J Eur Ceram Soc. 2019;39(14):4139–43.
23. Zhou DI, Randall CA, Pang L-X, Wang H, Guo J, Zhang G-Q, et al. Microwave dielectric properties of Li_2WO_4 ceramic with ultra-low sintering temperature. J Am Ceram Soc. 2011;94(2):348–50.
24. Gheisari R, Chamberlain H, Chi-Tangyie G, Zhang S, Goulas A, Lee CK, et al. Multi-material additive manufacturing of low sintering temperature $Bi_2Mo_2O_9$ ceramics with Ag floating electrodes by selective laser burnout. Vir Phys Pro J. 2020;15(2):133–47.
25. Wang D, Zhang S, Wang GE, Vardaxoglou Y, Whittow W, Cadman D, et al. Cold sintered $CaTiO_3$-K_2MoO_4 microwave dielectric ceramics for integrated microstrip patch antennas. App Mater Today. 2020;18:100519.
26. Ji Y, Song K, Luo X, Liu B, Barzegar Bafrooei H, Wang D. Microwave dielectric properties of (1–x)Li_2MoO_4-xMg_2SiO_4 composite ceramics fabricated by cold sintering process. Fron Mater. 2019;6:256.
27. Maria J-P, Kang X, Floyd RD, Dickey EC, Guo H, Guo J, et al. Cold sintering: current status and prospects. J Mater Res. 2017;32(17):3205–18.
28. Zhou D, Pang LX, Wang DW, Reaney IM. Novel water-assisting low firing MoO_3 microwave dielectric ceramics. J Eur Ceram Soc. 2019;39(7):2374–8.
29. Induja IJ, Sebastian MT. Microwave dielectric properties of mineral sillimanite obtained by conventional and cold sintering process. J Eur Ceram Soc. 2017;37(5):2143–7.
30. Hong WB, Li L, Cao M, Chen XM. Plastic deformation and effects of water in room-temperature cold sintering of NaCl microwave dielectric ceramics. J Am Ceram Soc. 2018;101(9):4038–43.
31. Vaataja M, Kahari H, Juuti J, Jantunen H. Li_2MoO_4-based composite ceramics fabricated from temperature- and atmosphere-sensitive MnZn ferrite at room temperature. J Am Ceram Soc. 2017;100(8):3626–35.
32. Guo J, Baker AL, Guo HZ, Lanagan M, Randall CA. Cold sintering process: a new era for ceramic packaging and microwave device development. J Am Ceram Soc. 2017;100(2):669–77.
33. Kahari H, Teirikangas M, Juuti J, Jantunen H. Dielectric properties of lithium molybdate ceramic fabricated at room temperature. J Am Ceram Soc. 2014;97(11):3378–9.
34. Liu Y, Liu P, Hu CX. Low-temperature preparation and microwave dielectric properties of cold sintered $Li_2Mg_3TiO_6$ nanocrystalline ceramics. Ceram Int. 2018;44(17):21047–52.
35. Guo J, Berbano SS, Guo HZ, Baker AL, Lanagan MT, Randall CA. Cold sintering process of composites: bridging the processing temperature gap of ceramic and polymer materials. Adv Funct Mater. 2016;26(39):7115–21.
36. Kahari H, Teirikangas M, Juuti J, Jantunen H. Room-temperature fabrication of microwave dielectric Li_2MoO_4-TiO_2 composite ceramics. Ceram Int. 2016;42(9):11442–6.
37. Faouri SS, Mostaed A, Dean JS, Wang D, Sinclair DC, Zhang S, et al. High quality factor cold sintered Li_2MoO_4-$BaFe_{12}O_{19}$ composites for microwave applications. Acta Mater. 2019;166:202–7.
38. Wang DW, Zhou D, Zhang SY, Vardaxoglou Y, Whittow WG, Cadman D, et al. Cold-sintered temperature stable

$Na_{0.5}Bi_{0.5}MoO_4$-Li_2MoO_4 microwave composite ceramics. Acs Sustain Chem Eng. 2018;6(2):2438–44.
39. Guo J, Guo H, Baker AL, Lanagan MT, Kupp ER, Messing GL, et al. Cold sintering: a paradigm shift for processing and integration of ceramics. Angew Chem Int Edit. 2016;55(38):11457–61.
40. Wang DW, Zhou D, Song KX, Feteira A, Randall CA, Reaney IM. Cold-sintered C0G multilayer ceramic capacitors. Adv Electron Mater. 2019;5(7):1900025.
41. Wang D, Zhang S, Zhou DI, Song K, Feteira A, Vardaxoglou Y, et al. Temperature stable cold sintered $(Bi_{0.95}Li_{0.05})(V_{0.9}Mo_{0.1})O$-$_4$-$Na_2Mo_2O_7$ microwave dielectric composites. Materials. 2019;12(9):1370.
42. Guo J, Zhao X, Herisson De Beauvoir T, Seo J-H, Berbano SS, Baker AL, et al. Recent progress in applications of the cold sintering process for ceramic-polymer composites. Adv Funct Mater. 2018;28(39):1801724.
43. Wang D, Siame B, Zhang S, Wang GE, Ju X, Li J, et al. Direct integration of cold sintered, temperature-stable $Bi_2Mo_2O_9$-K_2MoO_4 ceramics on printed circuit boards for satellite navigation antennas. J Eur Ceram Soc. 2020;40(12):4029–34
44. https://www.imoa.info/molybdenum/molybdenum-market-information.php. in. International Molybdenum Association.
45. http://www.metalary.com/molybdenum-price/. in. Metalary.
46. https://marketrealist.com/2016/06/dap-prices-trended-last-week/. in. Indexmundi.
47. https://www.indexmundi.com/commoditie s/?commodity=rock-phosphate. in. Indexmundi.
48. Seo J-H, Guo J, Guo H, Verlinde K, Heidary DSB, Rajagopalan R, et al. Cold sintering of a Li-ion cathode: $LiFePO_4$-composite with high volumetric capacity. Ceram Int. 2017;43(17):15370–4.
49. Sebastian MT, Jantunen H. Low loss dielectric materials for LTCC applications: a review. Int Mater Rev. 2008;53(2):57–90.
50. Garcia-Moreno O, Alvarez-Vega M, Garcia-Alvarado F, Garcia-Jaca J, Gallardo-Amores J, Sanjuán M, et al. Influence of the structure on the electrochemical performance of lithium transition metal phosphates as cathodic materials in rechargeable lithium batteries: a new high-pressure form of $LiMPO_4$ (M= Fe and Ni). Chem Mater. 2001;13(5):1570–6.
51. Kalinkin M, Abashev R, Zabolotskaya E, Baklanova I, Surdo A, Kellerman D. Paramagnetic surface defects in $LiMgPO_4$. Mater Res Exp. 2019;6:046206.

SUPPORTING INFORMATION

Additional supporting information may be found online in the Supporting Information section.

How to cite this article: Wang D, Chen J, Wang G, et al. Cold sintered $LiMgPO_4$ based composites for low temperature co-fired ceramic (LTCC) applications. *J Am Ceram Soc*. 2020;103:6237–6244. https://doi.org/10.1111/jace.17320